



ELSEVIER

Contents lists available at ScienceDirect

## Advances in Biological Regulation

journal homepage: [www.elsevier.com/locate/jbior](http://www.elsevier.com/locate/jbior)

# Biophysical approaches promote advances in the understanding of von Willebrand factor processing and function

Achim Löff<sup>a</sup>, Jochen P. Müller<sup>a</sup>, Martin Benoit<sup>a</sup>, Maria A. Brehm<sup>b,\*</sup><sup>a</sup> Department of Physics and Center for NanoScience, LMU Munich, Munich, Germany<sup>b</sup> Department of Pediatric Hematology and Oncology, University Medical Center Hamburg-Eppendorf, Hamburg, Germany

## ARTICLE INFO

## Article history:

Received 1 September 2016

Accepted 19 September 2016

Available online 28 September 2016

## Keywords:

von Willebrand factor

Dimerization

Biophysics

Atomic force microscopy

Single-molecule force spectroscopy

## ABSTRACT

The large multimeric plasma glycoprotein von Willebrand factor (VWF) is essential for primary hemostasis by recruiting platelets to sites of vascular injury. VWF multimers respond to elevated hydrodynamic forces by elongation, thereby increasing their adhesiveness to platelets. Thus, the activation of VWF is force-induced, as is its inactivation. Due to these attributes, VWF is a highly interesting system from a biophysical point of view, and is well suited for investigation using biophysical approaches. Here, we give an overview on recent studies that predominantly employed biophysical methods to gain novel insights into multiple aspects of VWF: Electron microscopy was used to shed light on the domain structure of VWF and the mechanism of VWF secretion. High-resolution stochastic optical reconstruction microscopy, atomic force microscopy (AFM), microscale thermophoresis and fluorescence correlation spectroscopy allowed identification of protein disulfide isomerase isoform A1 as the VWF dimerizing enzyme and, together with molecular dynamics simulations, postulation of the dimerization mechanism. Advanced mass spectrometry led to detailed identification of the glycan structures carried by VWF. Microfluidics was used to illustrate the interplay of force and VWF function. Results from optical tweezers measurements explained mechanisms of the force-dependent functions of VWF's domains A1 and A2 and, together with thermodynamic approaches, increased our understanding of mutation-induced dysfunctions of platelet-binding. AFM-based force measurements and AFM imaging enabled exploration of intermonomer interactions and their dependence on pH and divalent cations.

These advances would not have been possible by the use of biochemical methods alone and show the benefit of interdisciplinary research approaches.

© 2016 Elsevier Ltd. All rights reserved.

## Contents

1. Introduction .....	82
2. VWF structure, storage and secretion visualized by electron microscopy .....	83
3. Comprehensive biophysical investigation of VWF dimerization .....	84
3.1. Visualization of PDIA1-VWF complexes by STORM and AFM .....	84

\* Corresponding author.

E-mail address: [m.brehm@uke.de](mailto:m.brehm@uke.de) (M.A. Brehm).<http://dx.doi.org/10.1016/j.jbior.2016.09.010>

2212-4926/© 2016 Elsevier Ltd. All rights reserved.

3.2.	Binding affinity measurements using MST and FCS .....	84
3.3.	Mechanism of VWF dimerization modeled by docking and molecular dynamics (MD) simulations .....	85
4.	Characterization of VWF glycosylation by mass spectrometry .....	85
5.	Shear-induced globule-stretch transition of VWF in a microfluidic flow chamber .....	85
6.	Characterization of the A1-GPIIb $\alpha$ interaction by optical tweezers .....	86
7.	Unfolding and enzymatic cleavage of VWF's A2 domain in optical tweezers measurements .....	86
8.	Characterization of pH-dependent intermonomer interactions governing VWF's structure and mechanics .....	87
8.1.	AFM-based single-molecule force measurements on VWF dimers .....	87
8.2.	Investigation of the conformational ensemble of VWF dimers by AFM and small-angle X-ray scattering .....	87
9.	Biophysical investigation of von Willebrand disease mechanisms .....	88
10.	Conclusion .....	89
	Conflict of interest .....	89
	Acknowledgements .....	89
	References .....	89

## 1. Introduction

The best-described function of the multimeric glycoprotein von Willebrand factor (VWF) is its role in primary hemostasis. At sites of vascular injury, where conditions of elevated hydrodynamic forces are present, VWF recruits platelets to the damaged endothelium. Efficient binding of VWF to platelets correlates with the transition of VWF molecules from a rather globular to an elongated “string”-like conformation (Ruggeri et al., 2006; Schneider et al., 2007). The string-like structure of VWF results from its linear multimeric nature. VWF multimers are formed exclusively in endothelial cells (ECs) and megakaryocytes – the precursor cells of platelets. First, in the endoplasmic reticulum (ER), two single VWF molecules (= monomers; subdomains are schematically shown in Fig. 1A) are connected to dimers via C-terminal disulfide bonds (Fig. 1B). Only dimers proceed into the Golgi apparatus where they are N-terminally linked by interdimer disulfide bonds between the D'D3 domains (Wagner, 1990), resulting in multimers that consist of two to more than 40 dimeric subunits. Using a multi-lateral approach involving quantitative gel analysis, fluorescence correlation spectroscopy, and total internal reflection fluorescence microscopy it was recently shown that VWF multimer size follows an exponential size distribution (Lippok et al., 2013). The multimers become compacted and are stored in storage organelles called Weibel-Palade bodies (WPB's) in ECs (Wagner et al., 1982) and  $\alpha$ -granules in platelets (Jeanneau et al., 1984; Zucker et al., 1979). VWF can be secreted from these organelles upon extracellular stimuli (Fernandez et al., 1982; Loesberg et al., 1983; Miyata and Ruggeri, 1999; Sporn et al., 1989), and, while still attached to the cell, can elongate in the bloodstream (Ruggeri et al., 2006; Schneider et al., 2007). The transition from a compact into a stretched conformation leads to the activation of VWF's A1 domain to bind platelets. Remarkably, also the down-regulation of VWF's hemostatic activity – achieved by the cleavage of long VWF multimers into shorter, hemostatically less active ones – is force-induced, as the specific cleavage site is buried within VWF's A2 domain and exposed by unfolding of this domain (Zhang et al., 2009). Constitutively secreted, soluble VWF travels the circulation in a rather globular conformation. In addition to the abovementioned roles of VWF, this soluble VWF also fulfills a force-independent function as a transporter of coagulation factor VIII, which is thereby protected from degradation (Bennett et al., 1972).

The importance of VWF for primary hemostasis is illustrated by von Willebrand Disease (VWD), the most common hereditary bleeding disorder, which arises from a variety of mutations in the VWF gene (reviewed in Sadler, 1998). Three types of VWD have been defined: While type 1 is characterized by low levels of functional VWF, patients with type 3 have virtually no VWF in their plasma and platelets. In VWD type 2, VWF exhibits structural and functional defects (Sadler et al., 2006). Type 2 is further divided into subtypes 2A, 2B, 2M and 2N. VWD 2A is associated with a significant reduction of VWF high molecular weight multimers (HMWM) resulting in deficits in platelet-dependent function of VWF. 2M shows a similar phenotype, although HMWM are present at almost normal levels. 2B exhibits lack of HMWM due to enhanced VWF proteolysis and increased platelet binding, which often leads to strongly reduced platelets counts (thrombocytopenia). In subtype 2N, mutations diminish factor VIII binding, leading to a phenotype similar to hemophilia A (Schneppenheimer and Budde, 2011).

Further studies have revealed that VWF is also involved in arterial (Spiel et al., 2008) and venous thrombosis (Takahashi et al., 2009) as well as stroke (Kleinschnitz et al., 2009; Nieswandt and Stoll, 2010; Zhao et al., 2009). VWF has been described as a negative regulator of angiogenesis (Starke et al., 2011), and is able to stimulate smooth muscle cell proliferation (Bosmans et al., 1997; Qin et al., 2003). Moreover, VWF contributes to platelet and tumor cell apoptosis (Baud'huin et al., 2009) as well as to inflammatory processes (Bernardo et al., 2005; Denis et al., 2001; Petri et al., 2010), and it influences physiological bone remodeling via its interaction with osteoprotegerin (Shahbazi et al., 2007).

Key to VWF's functional diversity are its highly complex multi-domain structure and its extraordinary responsiveness to external forces, which in the vasculature result from the interplay of VWF's length with hydrodynamic flow (Springer, 2014). Both VWF's size (multimers can reach more than 20,000 kDa) and the importance of force-induced conformational changes for its function make this protein a highly interesting system from a biophysical point of view and an ideal research object for biophysical techniques. Recently, a variety of biophysical methods have been employed to investigate diverse aspects of VWF.

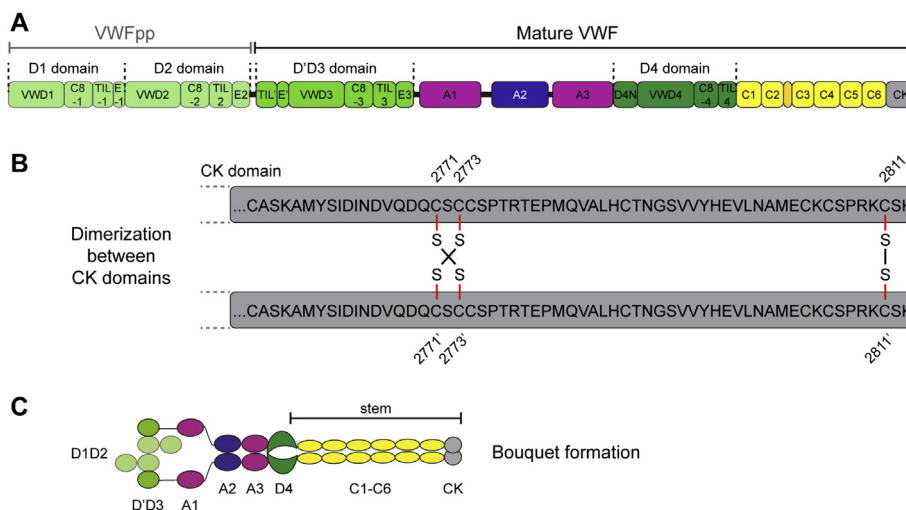


**Fig. 1. VWF domain structure.** (A) Schematic representation of VWF's domain structure, (B) dimerizing disulfide bonds between the CK domains of two VWF monomers and (C) dimeric bouquet formation.

These methods involve hydrodynamic and thermodynamic approaches, single-molecule manipulation and imaging techniques, optical microscopy, mass spectrometry, and computational modeling and simulation.

In this article, we give an overview on recent studies that predominantly used biophysical methods to gain novel insights into VWF structure, processing, packaging, storage, secretion, dynamics, function and dysfunction.

## 2. VWF structure, storage and secretion visualized by electron microscopy

All functions of a protein are defined by its tertiary structure, which allows interaction with other biomolecules for e.g. transport and regulation, and to fulfill its catalytic and non-catalytic functions. Thus, knowledge of a protein's tertiary structure is of paramount importance to understand all its functions. The primary structure can, to a certain degree, be used to predict the tertiary structure. Experimental approaches must then be used to confirm the prediction. Fundamental work by several groups on the determination of the sequence, disulfide connectivity and domain structure of VWF resulted in the following domain designation that was predominantly used in the literature: D1-D2-D'D3-A1-A2-A3-D4-B1-B2-B3-C1-C2-CTCK (Bonthron et al., 1986; Mancuso et al., 1989; Marti et al., 1987; Meitinger et al., 1993; Sadler et al., 1985; Shelton-Inloes et al., 1986; Titani et al., 1986; Verweij et al., 1986). The group of T.A. Springer recently re-annotated the domain boundaries of VWF by combining annotations on VWF in databases, knowledge on disulfide linkage and structural information of homologous domains with further sequence analysis (Zhou et al., 2012). The assigned domain modules were related to structure using transmission electron microscopy (TEM). This technique takes advantage of the short wavelength of the used electrons, which increases the obtained resolution by more than a factor of 100 compared to conventional light microscopy (Bozzola and Russell, 1999). Zhou et al. used different truncated, dimeric and monomeric, VWF constructs to dissect VWF's structure at a subdomain level (Zhou et al., 2011, 2012). This approach allowed them to suggest the following domain structure: D1-D2-D'D3-A1-A2-A3-D4-C1-C2-C3-C4-C5-C6-CK (Zhou et al., 2012) (Fig. 1A). While the D1-D2 domains represent the VWF propeptide (741 amino acids, VWFpp, Fig. 1A) that is cleaved off by furin, the mature VWF contains the domains D'D3 through CK (2050 amino acids, Fig. 1A). The EM studies further revealed that the D regions are assemblies, composed of smaller modules or lobes: The D1, D2, and D3 domains each are divided into VWD, C8, TIL, and E modules. D4 does not contain an E segment but instead the module D4N, which is not present in the other D assemblies. D' only consists of subdomains TIL' and E' (Zhou et al., 2012) (Fig. 1A).

EM studies were also employed to show that at the acidic pH values within the Golgi apparatus and WPB's, VWF dimers adopt a rather compact conformation, with the C-terminal portions of the two constituent monomers forming a "stem" (Fig. 1C) (Zhou et al., 2012). These stems are thought to be important for orderly linear multimerization and tubule formation for multimer storage in WPB's. In studies by the groups of J.E. Sadler and D.F. Cutler, EM was employed to shed light on the mechanism of tubule assembly. They showed that just the D1D2-propeptide and D'D3 dimers are sufficient for tubule formation (Huang et al., 2008; Michaux et al., 2006). The core of the tubule is built by a right-handed helix containing approximately four repeating units per turn. Each of these units consists of the propeptides positioned between two D'D3 domains of one dimer (Huang et al., 2008) (schematically shown in context of full-length VWF in Fig. 1C). The low pH and the high  $\text{Ca}^{2+}$  concentration (Michaux et al., 2006; Vischer and Wagner, 1994) in the Golgi increases the affinity of binding between D1D2 and D'D3, facilitating intersubunit disulfide bond formation for multimerization by bringing the two D3 domains in close proximity. The growing multimers then organize into helical tubules, with the stems directed outwards comprising

the matrix that later surrounds the denser tubules within WPB's (Huang et al., 2008). J. Eikenboom's group performed state-of-the-art correlative light and electron microscopy as well as electron tomography to investigate the biogenesis of WPB's and VWF secretion. These data provided intriguing information on how immature WPB's recruit more VWF and how mature WPB's can fuse to secretory pods before the release of VWF (Valentijn et al., 2011, 2008, 2010).

Overall, the EM studies led to a more detailed understanding of VWF's domain architecture, and helped to gain further insights into the mechanisms of VWF's multimerization and storage, as well as its secretion.

### 3. Comprehensive biophysical investigation of VWF dimerization

The first step of multimerization is the dimerization of VWF. It has been known for about 20 years that VWF is dimerized by the formation of disulfide bonds between cysteine residues in the C-terminal cystine-knot (CK) domain. The participating cysteines have been identified to be Cys2771, Cys2773 and Cys2811 (Fig. 1B) (Katsumi et al., 2000; Zhou and Springer, 2014) and cysteine mutations at positions 2771 (Enayat et al., 2001) and 2773 (Schneppenheim et al., 1996) were shown to be associated with dimerization defects in VWD type 2A. However, until recently the enzyme that catalyzes the reaction had not yet been identified.

Since dimerization occurs within the ER at neutral pH, it requires an ER-localized member of the thiol-disulfide oxidoreductase family. The protein disulfide isomerase PDI is able to catalyze oxidation, reduction and isomerization of disulfide bonds. To prove ER-localization of VWF in immunofluorescence studies, it has previously been described that VWF colocalizes with PDI isoform A1 (PDIA1) in the ER (Michaux et al., 2003). We thus suggested that this colocalization might have a physiological function, namely catalysis of VWF dimerization by PDIA1. Since attempts to prove this hypothesis by using standard biochemical approaches failed, we employed several high-resolution biophysical methods (Lippok et al., 2016) to unravel this secret.

#### 3.1. Visualization of PDIA1-VWF complexes by STORM and AFM

If PDIA1 was the enzyme in question, the dimerization reaction would require PDIA1 to interact with two VWF monomers in the ER. We used stochastic optical reconstruction microscopy (STORM) to visualize colocalization of VWF dimers and PDIA1. This method provides a much higher resolution than standard fluorescence microscopy as it overcomes the diffraction limit. In contrast to standard fluorescence microscopy, which uses constantly emitting fluorophores, STORM is based on high-accuracy localization of photo-switchable fluorophores. In each imaging cycle, only a fraction of fluorophores are turned on. The fluorophore positions are subsequently calculated from a series of imaging cycles allowing reconstruction of the overall image. Thereby an imaging resolution of less than 20 nm can be achieved (Rust et al., 2006).

Employing this method, we indeed found VWF clusters with the appropriate size for a dimer (~200 nm) (Zhou et al., 2011) exhibiting a single PDIA1 molecule bound in a central position (Lippok et al., 2016). This finding indicated that PDIA1 is involved in disulfide bond formation within VWF but did not allow for distinguishing between the formation of intramolecular bonds, which would support protein folding, and intermolecular bonds between CK domains, which would mediate the formation of dimers.

To determine if PDIA1 binds to the CK domain of VWF, we employed atomic force microscopy (AFM) in tapping mode to image VWF dimers co-adsorbed with PDIA1 onto a functionalized mica surface. AFM is a variant of scanning probe microscopy (SPM), and data are collected by scanning a sample surface with a mechanical probe (cantilever) that acts as a soft spring and possesses a sharp tip with a radius in the order of a few nanometers (Bhushan, 2010). Forces acting on the cantilever due to interactions between the sample surface and the tip can be detected as a deflection of the cantilever. In tapping mode (Fig. 3A), the cantilever is driven to oscillate at a constant frequency so that the tip only intermittently touches the sample surface during each oscillation cycle (Martin et al., 1987). Thus, lateral forces exerted on the sample during scanning are greatly reduced, making this imaging mode suitable also for soft and delicate biological samples such as proteins. The oscillation amplitude is monitored and kept constant by a feedback loop adjusting the z-position of the sample.

This information is converted into an image of the topography of the sample surface at a very high resolution. Here, the height of the sample is usually displayed as a pseudo-color plot (an exemplary image is shown in Fig. 3B). Using AFM, we imaged individual VWF dimers in the presence and absence of PDIA1 and were able to demonstrate that single PDIA1 molecules can form a complex with the CK domains of VWF dimers (Lippok et al., 2016).

#### 3.2. Binding affinity measurements using MST and FCS

To prove specific and direct interaction between VWF CK domains and PDIA1 *in vitro*, we used microscale thermophoresis (MST) and fluorescence correlation spectroscopy (FCS).

MST is the directed movement of molecules along a temperature gradient. Measurements are usually performed using a fluorescence microscope and a fluorescently labeled protein of interest. A heat gradient is induced by an infrared laser and movement of the protein out of the heat is detected by the decrease of the fluorescence signal. This method can be used to determine binding affinities between two proteins because the thermophoretic properties of a protein depend on its size, charge, conformation and solvation entropy, which change in case a binding partner is attached (de Groot and Mazur, 1984; Duhr and Braun, 2006; Lippok et al., 2012; Wienken et al., 2010).

FCS measures the dynamics of fluorescently labeled molecules diffusing in and out of a confocal volume due to Brownian motion. Here, the time-dependent fluctuations of the fluorescence intensity are analyzed (Elson and Magde, 1974; Magde et al., 1972, 1974; Petrov and Schwill, 2008; Rigler et al., 1993), which again differ between the bound and the unbound state of a protein and its binding partner.

We measured binding of purified recombinant wildtype VWF and fluorescently labeled PDIA1 and determined the dissociation constants by MST and FCS to be  $K_D = 236 \pm 66$  nM and  $K_D = 282 \pm 123$  nM, respectively. These data proved a direct and specific interaction of intermediate strength. Our finding that binding of PDI to the isolated CK domain of VWF exhibited a similar dissociation constant ( $K_D$  of  $258 \pm 104$  nM) showed that PDIA1 directly and exclusively binds to the CK domain of VWF and not to any other domain. Since dimerization is facilitated by disulfide bond formation between cysteines in the CK domain, these data indicated that PDIA1 is involved in VWF dimerization (Lippok et al., 2016).

### 3.3. Mechanism of VWF dimerization modeled by docking and molecular dynamics (MD) simulations

Computational approaches can be used for theoretical studies of biological molecules. Protein docking simulations can model protein-protein interactions at an atomic level and molecular dynamics (MD) simulations calculate the time-dependent behavior of a molecular system.

Combined with the above-described data and colocalization studies of von Willebrand Disease-associated VWF mutants, these methods allowed us to propose the following mechanism of VWF dimerization:

An initial electrostatic association between PDIA1 and VWF occurs N-terminally of amino acid residue 2772. Subsequently, an oxidized PDIA1 molecule forms a disulfide bond between its catalytic residue Cys36 and either Cys2771 or Cys2773 in the VWF monomer. After catalyzing the formation of the first disulfide bond (either Cys2771-2773' or Cys2771'-2773, no preference could be predicted), PDIA1 is released in its reduced form. The second bond (either Cys2771-2773' or Cys2771'-2773, depending on which one was formed first) is then formed by a new oxidized PDIA1 molecule. The presence of these two disulfide bridges leads to stabilization of the CK dimer and the CK C-termini can now assemble into a  $\beta$ -sheet conformation, which brings Cys2811 and Cys2811' in close proximity and enables formation of the third bond Cys2811-2811'. The simulation data suggest that the latter bond could also be formed by a spontaneous process or through catalysis by a different enzyme or a small molecule like glutathione. We hypothesized that disulfide bond Cys2811-2811' forms as a protective cover that shields the cysteine residues Cys2771 and Cys2773 from reduction by PDIA1, thereby ensuring VWF dimerization to be permanent (Lippok et al., 2016).

## 4. Characterization of VWF glycosylation by mass spectrometry

After leaving the ER, VWF dimers are multimerized in the Golgi apparatus. During their passage through this cellular compartment VWF becomes heavily glycosylated. To determine the detailed composition of the attached glycan structures, different groups employed advanced mass spectrometry (MS). A mass spectrometer determines the mass of a molecule by measuring the mass-to-charge ratio of its ions. To perform MS measurements, the molecule of interest is first ionized and the generated ions are electrostatically or magnetically directed into a mass analyzer where they are separated according to their mass-to-charge ratio and detected. The result is a spectrum derived from molecular ionization, ion separation, and ion detection that provides information on molecular mass and structure (Dass, 2001). Extending the work of previous studies (Matsui et al., 1992; Samor et al., 1982, 1989), Canis et al. and Solecka et al. determined the complete VWF N-glycan and O-glycan population using MALDI-TOF-MS (Matrix Assisted Laser Desorption/Ionization - Time of Flight - Mass Spectrometry) and tandem MS analysis (Canis et al., 2010, 2012; Solecka et al., 2016). Glycomics analyses identified about 100 distinct N-glycan compositions exhibiting a variety of structural features, including lactosaminic extensions, ABH blood group antigens and sulfated antennae, as well as bisecting and terminal GlcNAc residues resulting in about 300 different N-glycan structures (Canis et al., 2012). Analysis of the O-glycome revealed eighteen O-glycan structures including both core 1 and core 2 structures, unusual tetrasialylated core 1 O-glycans and ABH antigen-containing core 2 O-glycans (Canis et al., 2010). Glycan structures present blood group determinants on VWF and influence VWF clearance and proteolysis. Thus, knowledge of the detailed glycosylation pattern of VWF lays ground for further studies to elucidate the association between the ABO blood group and VWF plasma concentration and the detailed mechanism of VWF clearance as well as control of plasma VWF multimer size.

## 5. Shear-induced globule-stretch transition of VWF in a microfluidic flow chamber

After complete posttranslational modification and storage, VWF multimers are secreted from the synthesizing cell when their function in primary hemostasis is required. Fundamental work by Z.M. Ruggeri's group has shown that, remarkably, platelet aggregation can be induced by VWF without prior signaling-induced activation of platelets when shear rates exceed a critical threshold (Ruggeri et al., 2006). This phenomenon requires VWF bound to the surface as well as soluble VWF. The exact molecular mechanisms that underlie this force-induced activation of platelet binding to VWF have not yet been fully elucidated. However, it is established that binding of platelets to VWF under high shear conditions depends on the interaction between VWF's A1 domain and the glycoprotein (GP) Ib $\alpha$  subunit (GPIb $\alpha$ ) on the platelet surface (Miyata and Ruggeri, 1999; Reininger et al., 2006; Ruggeri et al., 2006).

A critical contribution to comprehend the interplay of force and VWF's function was made by Schneider et al., who studied the impact of shear flow on the conformation and adhesive properties of single VWF fibers (Schneider et al., 2007). Schneider et al. utilized a microchannel structure on top of a thin transparent piezoelectric material as a miniaturized flow chamber with an integrated surface acoustic wave (SAW) pump (Guttenberg et al., 2004). A SAW pump generates a directed surface wave by applying an alternating voltage pattern to appropriately patterned electrodes on the piezoelectric material, which periodically slightly deforms in response to the applied voltage. At drive frequencies in the MHz regime, these waves couple to liquid, causing acceleration of the latter, thus allowing for microfluidic experiments in small volume geometries. By combining this microfluidic device with an inverted fluorescence microscope, it became possible not only to observe individual, fluorescently labeled, floating VWF multimers, but also their interaction with surface-bound substrates at high shear rates (Schneider et al., 2007). Strikingly, binding of VWF to immobilized collagen was essentially only observed above a critical shear rate of approximately 5000/s. In addition, in experiments without adhesive surfaces, fluorescently labeled VWF multimers were observed to abruptly change their conformation from an overall globular into a stretched one, remarkably at the same critical shear rate of ~5000/s. This transition was reversible, since the protein immediately returned to its compact conformation when the shear rate was reduced. The abrupt shear-induced elongation behavior could be reproduced in simple simulations, which coarse-grained VWF monomers as spheres interacting with each other via a standard Lennard-Jones potential (Schneider et al., 2007). Overall, these observations suggested VWF fibers to be hydrodynamically activated biopolymers, being hemostatically active only under high shear rates by changing their adhesive properties upon force-induced conformational changes that render particular binding sites in VWF active.

While the cleavage of VWF's A2 domain had already been known to be shear-dependent (Dent et al., 1990; Tsai, 1996), the findings by Schneider et al. strongly suggested the function of VWF's adhesive domains to be force-regulated as well.

As described below, other groups subsequently used optical tweezers measurements and atomic force microscopy to investigate the interplay between force and VWF's function at the single-molecule level.

## 6. Characterization of the A1-GPIIb $\alpha$ interaction by optical tweezers

The shear-induced elongation of VWF activates binding of platelet GPIIb $\alpha$  to the A1 domain of VWF. Intriguing insights into the force dependence of this interaction at the single-molecule level have recently been gained by two optical tweezers (OT) studies by Kim et al. (Kim et al., 2010, 2015). OT make use of the strong electric field gradients occurring in a highly focused laser beam to trap dielectric particles, such as polystyrene beads (Ashkin et al., 1986). For single-molecule force measurements on biomolecules, the molecules of interest are usually coupled by specific interactions to the trapped bead with their one end and to a second bead that is held by a micropipette with their other end. By increasing the distance of the second bead from the trapped bead, force can be exerted on the molecule. This force can precisely be measured by monitoring the resulting small displacement of the trapped bead from the trap center.

In both studies Kim et al. utilized a sophisticated protein construct that combines VWF's A1 domain and GPIIb $\alpha$ , connected by a flexible polypeptide linker between the C-terminus of A1 and the N-terminus of GPIIb $\alpha$ , in a single molecule. This construct was attached to beads via DNA handles, subjected to force measurements, and binding and unbinding events of the receptor–ligand complex were monitored. Strikingly, two distinct states of the receptor–ligand bond were found, and switching between the two states was induced by force. While the first state was observed at low forces, the second state occurred at forces above ~10 pN and exhibited a markedly higher lifetime, corresponding to a lower off-rate (Kim et al., 2010). Moreover, the application of force was shown to also strongly enhance bond association kinetics by inducing switching to a faster on-rate (Kim et al., 2015). This finding of a force-induced switching of the A1-GPIIb $\alpha$  bond to a second state with both faster on-rate and longer lifetime – at physiologically relevant forces – provides an explanation for shear-enhanced binding of platelets to VWF. Importantly, in elongated VWF multimers, force propagates through the A1 domain very similarly to A1 in the unbound state of the A1-GPIIb $\alpha$  construct used for above measurements. In this construct however, also GPIIb $\alpha$  is loaded with force in the unbound state, in contrast to the situation *in vivo*, where GPIIb $\alpha$  on the platelet surface is not expected to experience significant forces before binding (Kim et al., 2015). Kim et al. consequently hypothesized that the existence of two bond states might originate from two distinct conformations of A1, although a second conformation has so far not been confirmed by crystal structures (Kim et al., 2010, 2015).

## 7. Unfolding and enzymatic cleavage of VWF's A2 domain in optical tweezers measurements

Not only VWF's activation, but also the down-regulation of VWF's hemostatic potential by cleavage of long multimers into shorter, hemostatically less active ones is a force-induced process. It relies on the specific metalloprotease ADAMTS13, which under high flow conditions can cleave the Tyr1605–Met1606 bond within VWF's A2 domain (Dent et al., 1990; Tsai, 1996). However, the detailed molecular mechanisms behind the force dependence of this cleavage in A2 have only recently been elucidated by force measurements using optical tweezers.

Zhang et al. employed this approach to investigate the force response of individual VWF A2 domains that were tethered to beads via DNA handles (Zhang et al., 2009). Force-induced unfolding of A2 domains was observed at forces of ~7–14 pN, at loading rates ranging from 0.35 to 350 pN/s, and repeatedly proceeded via an intermediate state. Importantly, A2 domain unfolding was reversible, and fast refolding was observed when clamping A2 at low forces below ~2 pN. The lifetime of the unfolded state at zero force was deduced to be in the order of 2 s.

Zhang et al. could further show that A2 unfolding is required for cleavage by ADAMTS13. Isolated A2 domains were unfolded in the presence of ADAMTS13 and subsequently clamped at a force of 5 pN to prevent fast refolding. Cleavage by ADAMTS13, detectable as a drop in force to zero, was indeed observed. For folded A2 domains at 5 pN, as well as for unfolded A2 domains in the absence of the enzyme, such force drops occurred only very scarcely. Based on the measured enzyme kinetics, the time scale for cleavage of an unfolded A2 domain at physiological concentrations of ADAMTS13 was estimated to be in the order of 200 s. The finding that this time scale is markedly longer than the lifetime of an unfolded A2 domain in the absence of force implies that over the short time periods relevant in hemostasis, VWF's hemostatic functions, i.e. binding to platelets and collagen, should win out over enzymatic cleavage of A2. Zhang et al. further provided estimations on the forces acting on a multimer in hydrodynamic flow. These estimations strongly suggest that the forces required for A2 unfolding will indeed be reached in the bloodstream, particularly under elevated elongational flow conditions, as for instance found at sites of vascular injury. As for longer multimers these forces are reached more readily than for shorter ones, the force-induced enzymatic cleavage of A2 domains presents a means to effectively control VWF's size distribution and to specifically cleave the longest, hemostatically most active VWF multimers.

Importantly, force-induced A2 unfolding was not only shown for isolated A2 domains, but also for A2 in the presence of neighboring domains (Ying et al., 2010). Ying et al. employed OT to stretch a protein construct consisting of three repeats of the triplet A1–A2–A3 domains, and observed A2 unfolding at similar, albeit slightly higher, forces compared with the case of an isolated A2 domain. This finding indicates that A2 unfolding is not significantly affected by its neighboring domains A1 and A3.

## 8. Characterization of pH-dependent intermonomer interactions governing VWF's structure and mechanics

### 8.1. AFM-based single-molecule force measurements on VWF dimers

In order to elucidate the molecular mechanisms underlying the force response of VWF in context of the full-length protein, the group of M. Benoit recently performed AFM-based single-molecule force measurements on VWF dimers, the smallest repeating subunits within VWF multimers (Müller et al., 2016b). To this end, recombinantly expressed dimers possessing two different peptide tags at the two N-termini of the dimer were used (Fig. 2A). The tags allowed for site-specific attachment of dimers to a functionalized glass surface and for specifically pulling these dimers in their native force-sensing direction via a functionalized AFM cantilever. Specific force–extension traces were identified by using the appearance of two A2 domain unfolding peaks as a positive fingerprint. Under near-physiological buffer conditions – at pH 7.4 and in the presence of divalent ions – two types of characteristic force–extension traces were obtained at roughly the same ratios: Traces of type II (Fig. 2C) only showed the two A2 unfolding signals, whereas traces of type I additionally exhibited a peak at comparably high forces above ~50 pN (Fig. 2B). This peak was shown to result from the dissociation of a strong intermonomer interaction that is mediated by VWF's D4 domain (Fig. 2D) and crucially relies on divalent ions. As this strong intermonomer interaction, which is present in roughly half of the dimers, initially shields ~80 nm of the length of a dimer, it will significantly decrease the effective length of VWF multimers. Consequently, as the forces acting on a multimer in hydrodynamic flow strongly correlate with multimer length, the strong intermonomer interaction can be expected to considerably affect VWF's force-sensing ability.

Müller et al. further showed that the ratio of type I force–extension traces, i.e. the ratio of dimers exhibiting the strong intermonomer interaction, possesses a pronounced pH dependence (Fig. 2E) (Müller et al., 2016a). This ratio was observed to be highest at pH 7.4, but to rapidly decrease upon lowering the pH, and type I traces were essentially never obtained at pH values below ~6.8. Also upon alkalization, the ratio of type I traces slightly decreased. These findings suggest highest mechanical resistance of VWF at physiological pH and a markedly reduced resistance even for minor pH changes. The authors therefore speculated that local pH deviations might represent a means to enhance VWF's hemostatic activity where needed, e.g. at sites of vascular injury.

### 8.2. Investigation of the conformational ensemble of VWF dimers by AFM and small-angle X-ray scattering

Complementarily to abovementioned force measurements, Müller et al. also investigated the conformations of individual VWF dimers adsorbed onto a functionalized mica surface by AFM imaging (Fig. 3A) (Müller et al., 2016b). In general, both compact and flexible conformations of dimers were observed, characterized by closed and (partially) open C-terminal stems, respectively (Fig. 3B). To assess the impact of varying pH and ionic conditions, Müller, Löff et al. further determined the ratio of compact dimers – defined as dimers possessing fully closed stems – as a function of the pH, both in the presence and in the absence of divalent ions, i.e. under conditions that enable and obstruct the strong intermonomer interaction, respectively (Fig. 3C) (Müller et al., 2016a). In the latter case, compactness of dimers monotonically increased with decreasing pH (Fig. 3C, red), in line with the abovementioned previous TEM study (Zhou et al., 2011). In the presence of divalent ions, however, a second regime of compactness was observed above pH values of ~6.8, reaching its maximum at pH 7.4 (Fig. 3C, blue). Together, the data from force and imaging experiments showed that compactness of dimers above pH ~6.8 is promoted by the strong intermonomer interaction, whereas compactness under acidic conditions must be mediated by another intermonomer interaction that is mechanically weaker. The findings from AFM imaging were further corroborated by results from small-angle X-ray scattering (SAXS) experiments performed under varying solution conditions. SAXS is a bulk technique that

gives information about the conformational ensemble of, e.g., biomolecules in solution based on their X-ray scattering intensity profiles obtained under low scattering angles (Lipfert and Doniach, 2007).

In AFM images of dimers with a deletion of the D4 domain, only a negligible number of compact dimers were observed throughout the whole pH range (Fig. 3C, brown), indicating that D4 is essential not only for the formation of the strong intermonomer interaction, but also for promoting compactness under acidic conditions. In other words, this suggests that the D4 domain mediates two intermonomer interactions that possess markedly different mechanical stabilities and exhibit opposite pH dependencies. While the strong intermonomer interaction can be expected to markedly tune VWF's force-sensing ability (Müller et al., 2016a, 2016b), the weak interaction under acidic conditions can be assumed to be important for orderly multimerization and storage of VWF (Zhou et al., 2011).

## 9. Biophysical investigation of von Willebrand disease mechanisms

The above-described studies focused primarily on elucidating basic scientific questions with respect to VWF's structure and force responsiveness, but biophysical approaches are also more and more used to elucidate the mechanisms underlying different VWD subtypes.

For example, a focus of M. Auton's group is to elucidate the mechanisms of VWD 2B and 2M phenotypes. They have surveyed the effects of 16 VWD-associated mutations on the structure and rheology of the VWF A1 domain adhesiveness to GPIIb $\alpha$ . These mutations cause a dynamic phenotypical range in the severity of bleeding. The bleeding tendencies can be induced by reduced binding of VWF to platelets (loss-of-function mutations) or thrombocytopenia induced by enhanced platelet binding to VWF harboring gain-of-function mutations. Tischer et al. have used new rheological tools in combination with classical thermodynamic, biophysical, and spectroscopic metrics to establish a tendency of the A1 domain to fold to a so called pathological molten globule state, a conformation exhibiting the loss of the global tertiary structure while retaining secondary and potential supersecondary structure elements. Depending on the extent of these structural changes, an increasingly high affinity for GPIIb $\alpha$  was established that linearly correlates with firmness of the attachment of platelets under shear flow and severity of thrombocytopenia in the patients (Tischer et al., 2014). Conversely, this means that mutations that increase the rigidity of the A1 domain prevent transition into the GPIIb $\alpha$  binding state. This hypothesis was supported by a

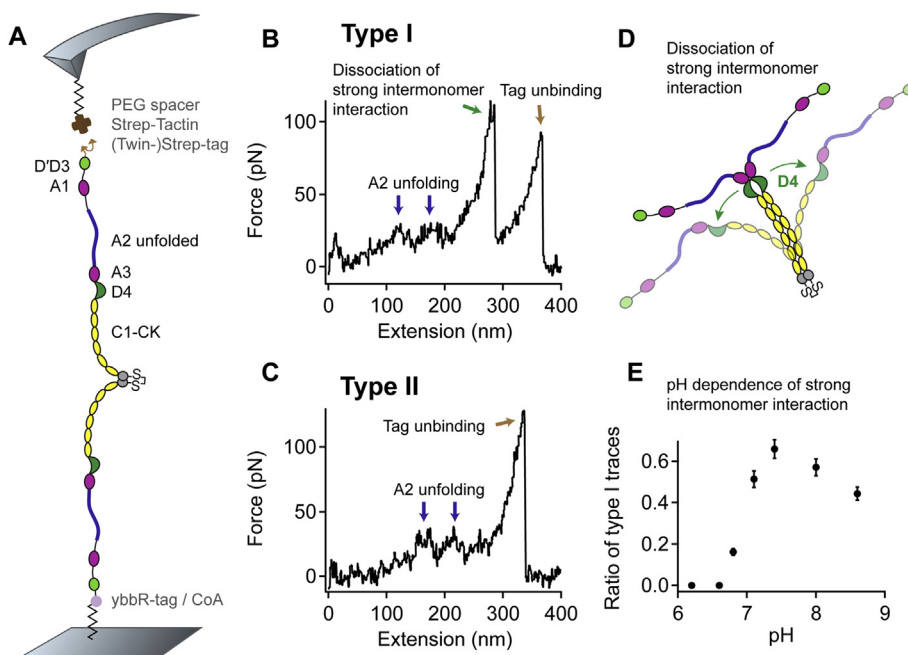


**Fig. 2.** AFM-based single-molecule force measurements on VWF dimers. (A) Schematic representation of AFM-based single-molecule force measurements on VWF heterodimers as performed by Müller et al. (Müller et al., 2016b). For covalent anchoring to a Coenzyme A (CoA) coated glass surface, a ybbR-tag was located at the N-terminus of one of the two constituent monomers. At the N-terminus of the other monomer, either a single Strep-tag or a Twin-Strep-tag was placed, enabling specific pulling via a Strep-Tactin functionalized cantilever. Polyethylene glycol (PEG) spacers were used at both glass surface and cantilever in order to avoid protein–surface interactions. (B and C) Denoised force–extension traces of type I and II characterized by the appearance of A2 unfolding peaks (blue arrows) at low (type I, B) and high (type II, C) extension values, respectively. In traces of type I an additional peak at higher force (green arrow) was observed. This peak was shown to result from the dissociation of a strong intermonomer interaction in dimers mediated by the D4 domain. The final peak (brown arrow) corresponds to the dissociation of the (Twin-)Strep-tag–Strep-Tactin interaction. (D) Illustration of the conformational changes of VWF dimers upon dissociation of the strong intermonomer interaction. (E) pH dependence of the strong intermonomer interaction, i.e. the ratio of type I traces as a function of the pH. Panels A–D appeared in similar form originally in (Müller et al., 2016b). Panel E appeared originally in (Müller et al., 2016a).

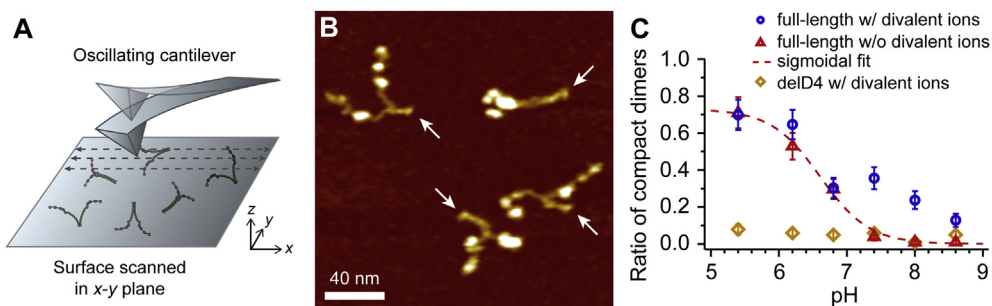


**Fig. 3. AFM imaging of VWF dimers.** (A) Schematic of AFM imaging in tapping mode. The AFM cantilever is driven to oscillate at a constant frequency. While the sample surface is scanned line-wise, the oscillation amplitude is monitored and kept constant by a feedback loop adjusting the z-position of the sample. This allows generating a topography map of the sample. (B) Representative AFM image of VWF dimers adsorbed onto a functionalized mica surface at near-physiological buffer conditions. Both compact (upper right dimer) and flexible conformations of dimers were observed. Arrows mark positions of CK domains. The range from the darkest to the lightest color corresponds to 2.4 nm. (C) Ratio of compact dimers, i.e. dimers possessing fully closed C-terminal stems, as a function of the pH. Shown are data for full-length dimers obtained in the presence (blue) and absence (red) of divalent ions, and data for dimers with a deletion of the D4 domain (delD4 dimers, brown) in the presence of divalent ions. The red dashed line is a sigmoidal fit to the data obtained in the absence of divalent ions. Panels B and C were adopted from (Müller et al., 2016b) and (Müller et al., 2016a), respectively.

recent study from the same group describing the effects of the rare type 2M VWD mutation p.Gly1324Ser that diminishes the platelet GPIIb $\alpha$  binding ability of the VWF A1 domain (Tischer et al., 2016). Tischer et al. found this mutation to enhance the thermodynamic stability and reduce the rate of unfolding. The crystal structure, which represents the conformation of the A1 domain in the absence of hydrodynamic force, was identical to the wildtype structure. The enhanced stability under flow thus appears to originate from the steric consequences of adding a side chain and an additional hydrogen bond to H1322 across the  $\beta$ 2- $\beta$ 3 hairpin in the GPIIb $\alpha$  binding interface of A1, which restrains the conformational degrees of freedom and the overall flexibility of the A1 domain (Tischer et al., 2016).

As mentioned above, the ability of the A1 domain to switch between different binding modes was also observed by Kim et al. who performed OT measurements to investigate the gain-of-function mutation p.Arg1306Gln, which causes VWD type 2B (Kim et al., 2015). At zero force (in the first bond state), the A1-R1306Q/GPIIb $\alpha$ -wildtype complex did not exhibit a marked difference in the association and dissociation kinetics compared to the A1-wildtype/GPIIb $\alpha$ -wildtype complex (Kim et al., 2015). Force-induced switching to the second bond state, however, resulted in a markedly faster bond formation compared with the wildtype, indicating an important role of force in this disease phenotype and again suggesting that the force regulation of the A1-GPIIb $\alpha$  interaction may play a central role in the activation of VWF for platelet binding.

## 10. Conclusion

In this review, we have given a brief overview of novel insights into diverse aspects of VWF that have predominantly been achieved by employing biophysical techniques.

These advances would not have been possible by the use of biochemical methods alone and show the benefit of interdisciplinary research approaches. In the age of translational science, we are becoming increasingly aware of the advantages of combining technologies from different disciplines, such as medicine, biochemistry, biophysics and structural biology in interdisciplinary approaches to increase our understanding of disease mechanisms. The obtained data are already being used - and most probably will be even more in the future - to develop novel treatment strategies and diagnostic tools to advance and optimize personalized patient care.

## Conflict of interest

The authors declare no conflict of interest.

## Acknowledgements

We thank all members of our interdisciplinary research group SHENC (DFG research group FOR1543: Shear flow regulation of hemostasis – bridging the gap between nanomechanics and clinical presentation, [www.shenc.de](http://www.shenc.de)) and the DFG (SCHN325/6-2 and BE4281/2-2) for financial support of some of the above-summarized studies.

## References

- Ashkin, A., Dziedzic, J.M., Bjorkholm, J.E., Chu, S., 1986. Observation of a single-beam gradient force optical trap for dielectric particles. *Opt. Lett.* 11, 288.
- Baud'huin, M., Duplomb, L., Teletchea, S., Charrier, C., Maillason, M., Fouassier, M., Heymann, D., 2009. Factor VIII-von Willebrand factor complex inhibits osteoclastogenesis and controls cell survival. *J. Biol. Chem.* 284, 31704–31713.

- Bennett, B., Ratnoff, O.D., Levin, J., 1972. Immunologic studies in von Willebrand's disease. Evidence that the antihemophilic factor (AHF) produced after transfusions lacks an antigen associated with normal AHF and the inactive material produced by patients with classic hemophilia. *J. Clin. Investig.* 51, 2597–2601.
- Bernardo, A., Ball, C., Nolasco, L., Choi, H., Moake, J.L., Dong, J.F., 2005. Platelets adhered to endothelial cell-bound ultra-large von Willebrand factor strings support leukocyte tethering and rolling under high shear stress. *J. Thromb. Haemost.* JTH 3, 562–570.
- Bhushan, B., 2010. Springer handbook of Nanotechnology. Springer, Berlin ; New York xlviii, 1961 p. pp.
- Bonthron, D.T., Handin, R.L., Kaufman, R.J., Wasley, L.C., Orr, E.C., Mitscock, L.M., Ewenstein, B., Loscalzo, J., Ginsburg, D., Orkin, S.H., 1986. Structure of Pre-Pro-von Willebrand factor and its expression in heterologous cells. *Nature* 324, 270–273.
- Bosmans, J.M., Kockx, M.M., Vrints, C.J., Bult, H., De Meyer, G.R., Herman, A.G., 1997. Fibrin(ogen) and von Willebrand factor deposition are associated with intimal thickening after balloon angioplasty of the rabbit carotid artery. *Arterioscler. Thromb. Vasc. Biol.* 17, 634–645.
- Bozzola, J.J., Russell, L.D., 1999. *Electron Microscopy : Principles and Techniques for Biologists*. Jones and Bartlett, Sudbury, Mass xxiii, 670 p. pp.
- Canis, K., McKinnon, T.A., Nowak, A., Haslam, S.M., Panico, M., Morris, H.R., Laffan, M.A., Dell, A., 2012. Mapping the N-glycome of human von Willebrand factor. *Biochem. J.* 447, 217–228.
- Canis, K., McKinnon, T.A., Nowak, A., Panico, M., Morris, H.R., Laffan, M., Dell, A., 2010. The plasma von Willebrand factor O-glycome comprises a surprising variety of structures including ABH antigens and disialosyl motifs. *J. Thromb. Haemost.* JTH 8, 137–145.
- Dass, C., 2001. *Principles and Practice of Biological Mass Spectrometry*. John Wiley, New York xxvii, 416 p. pp.
- de Groot, S.R., Mazur, P., 1984. *Non-equilibrium Thermodynamics*. Dover Publications, New York x, 510 p. pp.
- Denis, C.V., Andre, P., Saffaripour, S., Wagner, D.D., 2001. Defect in regulated secretion of P-selectin affects leukocyte recruitment in von Willebrand factor-deficient mice. *Proc. Natl. Acad. Sci. U. S. A.* 98, 4072–4077.
- Dent, J.A., Berkowitz, S.D., Ware, J., Kasper, C.K., Ruggeri, Z.M., 1990. Identification of a cleavage site directing the immunochemical detection of molecular abnormalities in type IIA von Willebrand factor. *Proc. Natl. Acad. Sci. U. S. A.* 87, 6306–6310.
- Duhr, S., Braun, D., 2006. Thermophoretic depletion follows Boltzmann distribution. *Phys. Rev. Lett.* 96, 168301.
- Elson, E.L., Magde, D., 1974. Fluorescence correlation spectroscopy. I. Conceptual basis and theory. *Biopolymers* 13, 1–27.
- Enayat, M.S., Guilliat, A.M., Surdhar, G.K., Jenkins, P.V., Pasi, K.J., Toh, C.H., Williams, M.D., Hill, F.G., 2001. Aberrant dimerization of von Willebrand factor as the result of mutations in the carboxy-terminal region: identification of 3 mutations in members of 3 different families with type 2a (phenotype iid) von Willebrand disease. *Blood* 98, 674–680.
- Fernandez, M.F., Ginsberg, M.H., Ruggeri, Z.M., Battle, F.J., Zimmerman, T.S., 1982. Multimeric structure of platelet factor VIII/von Willebrand factor: the presence of larger multimers and their reassociation with thrombin-stimulated platelets. *Blood* 60, 1132–1138.
- Guttenberg, Z., Rathgeber, A., Keller, S., Radler, J.O., Wixforth, A., Kostur, M., Schindler, M., Talkner, P., 2004. Flow profiling of a surface-acoustic-wave nanopump. *Phys. Rev. E Stat. Nonlinear, Soft Matter Phys.* 70, 056311.
- Huang, R.H., Wang, Y., Roth, R., Yu, X., Purvis, A.R., Heuser, J.E., Egelman, E.H., Sadler, J.E., 2008. Assembly of Weibel-Palade body-like tubules from N-terminal domains of von Willebrand factor. *Proc. Natl. Acad. Sci. U. S. A.* 105, 482–487.
- Jeanneau, C., Avner, P., Sultan, Y., 1984. Use of monoclonal antibody and colloidal gold in E.M. localization of von Willebrand factor in megakaryocytes and platelets. *Cell. Biol. Int. Rep.* 8, 841–848.
- Katsumi, A., Tuley, E.A., Bodo, I., Sadler, J.E., 2000. Localization of disulfide bonds in the cystine knot domain of human von Willebrand factor. *J. Biol. Chem.* 275, 25585–25594.
- Kim, J., Hudson, N.E., Springer, T.A., 2015. Force-induced on-rate switching and modulation by mutations in gain-of-function von Willebrand diseases. *Proc. Natl. Acad. Sci. U. S. A.* 112, 4648–4653.
- Kim, J., Zhang, C.Z., Zhang, X., Springer, T.A., 2010. A mechanically stabilized receptor-ligand flex-bond important in the vasculature. *Nature* 466, 992–995.
- Kleinschnitz, C., De Meyer, S.F., Schwarz, T., Austinat, M., Vanhoorelbeke, K., Nieswandt, B., Deckmyn, H., Stoll, G., 2009. Deficiency of von Willebrand factor protects mice from ischemic stroke. *Blood* 113, 3600–3603.
- Lipfert, J., Doniach, S., 2007. Small-angle X-ray scattering from RNA, proteins, and protein complexes. *Annu. Rev. Biophys. Biomol. Struct.* 36, 307–327.
- Lippok, S., Kolsek, K., Lof, A., Eggert, D., Vanderlinden, W., Muller, J.P., Konig, G., Obser, T., Rohrs, K., Schneppenheim, S., Budde, U., Baldauf, C., Aponte-Santamaria, C., Grater, F., Schneppenheim, R., Radler, J.O., Brehm, M.A., 2016. von Willebrand factor is dimerized by protein disulfide isomerase. *Blood* 127, 1183–1191.
- Lippok, S., Obser, T., Müller, J.P., Stierle, V.K., Benoit, M., Budde, U., Schneppenheim, R., Rädler, J.O., 2013. Exponential size distribution of von Willebrand factor. *Biophys. J.* 105, 1208–1216.
- Lippok, S., Seidel, S.A.I., Duhr, S., Uhland, K., Holthoff, H.-P., Jenne, D., Braun, D., 2012. Direct detection of antibody concentration and affinity in human serum using microscale thermophoresis. *Anal. Chem.* 84, 3523–3530.
- Loesberg, C., Gonsalves, M.D., Zandbergen, J., Willems, C., van Aken, W.G., Stel, H.V., Van Mourik, J.A., De Groot, P.G., 1983. The effect of calcium on the secretion of factor VIII-related antigen by cultured human endothelial cells. *Biochim. Biophys. Acta* 763, 160–168.
- Magde, D., Elson, E., Webb, W.W., 1972. Thermodynamic fluctuations in a reacting system - measurement by fluorescence correlation spectroscopy. *Phys. Rev. Lett.* 29, 705–708.
- Magde, D., Elson, E.L., Webb, W.W., 1974. Fluorescence correlation spectroscopy. II. An experimental realization. *Biopolymers* 13, 29–61.
- Mancuso, D.J., Tuley, E.A., Westfield, L.A., Worrall, N.K., Shelton-Inloes, B.B., Sorace, J.M., Alevy, Y.G., Sadler, J.E., 1989. Structure of the gene for human von Willebrand factor. *J. Biol. Chem.* 264, 19514–19527.
- Marti, T., Rosselet, S.J., Titani, K., Walsh, K.A., 1987. Identification of disulfide-bridged substructures within human von Willebrand factor. *Biochemistry* 26, 8099–8109.
- Martin, Y., Williams, C.C., Wickramasinghe, H.K., 1987. Atomic force microscope force mapping and profiling on a sub 100-Å scale. *J. Appl. Phys.* 61, 4723–4729.
- Matsui, T., Titani, K., Mizuochi, T., 1992. Structures of the asparagine-linked oligosaccharide chains of human von Willebrand factor. Occurrence of blood group A, B, and H(O) structures. *J. Biol. Chem.* 267, 8723–8731.
- Meitinger, T., Meindl, A., Bork, P., Rost, B., Sander, C., Haasemann, M., Murken, J., 1993. Molecular modelling of the Norrie disease protein predicts a cystine knot growth factor tertiary structure. *Nat. Genet.* 5, 376–380.
- Michaux, G., Abbitt, K.B., Collinson, L.M., Haberichter, S.L., Norman, K.E., Cutler, D.F., 2006. The physiological function of von Willebrand's factor depends on its tubular storage in endothelial Weibel-Palade bodies. *Dev. Cell.* 10, 223–232.
- Michaux, G., Hewlett, L.J., Messenger, S.L., Goodeve, A.C., Peake, I.R., Daly, M.E., Cutler, D.F., 2003. Analysis of intracellular storage and regulated secretion of 3 von Willebrand disease-causing variants of von Willebrand factor. *Blood* 102, 2452–2458.
- Miyata, S., Ruggeri, Z.M., 1999. Distinct structural attributes regulating von Willebrand factor A1 domain interaction with platelet glycoprotein Ibalpha under flow. *J. Biol. Chem.* 274, 6586–6593.
- Müller, J.P., Löf, A., Mielke, S., Obser, T., Bruetzel, L.K., Vanderlinden, W., Lipfert, J., Schneppenheim, R., Benoit, M., 2016a. pH-Dependent Interactions in Dimers Govern the Mechanics and Structure of von Willebrand Factor. *Biophys. J.* 111, 312–322.
- Müller, J.P., Mielke, S., Löf, A., Obser, T., Beer, C., Bruetzel, L.K., Pippig, D.A., Vanderlinden, W., Lipfert, J., Schneppenheim, R., Benoit, M., 2016b. Force sensing by the vascular protein von Willebrand factor is tuned by a strong intermonomer interaction. *Proc. Natl. Acad. Sci. U. S. A.* 113, 1208–1213.
- Nieswandt, B., Stoll, G., 2010. The smaller, the better: VWF in stroke. *Blood* 115, 1477–1478.
- Petri, B., Broermann, A., Li, H., Khandoga, A.G., Zarbock, A., Krombach, F., Goerge, T., Schneider, S.W., Jones, C., Nieswandt, B., Wild, M.K., Vestweber, D., 2010. Von Willebrand factor promotes leukocyte extravasation. *Blood* 116, 4712–4719.
- Petrov, E.P., Schwille, P., 2008. State of the art and novel trends in fluorescence correlation spectroscopy. *Stand. Qual. Assur. Fluoresc. Meas.* II 145–197.

- Qin, F., Impeduglia, T., Schaffer, P., Dardik, H., 2003. Overexpression of von Willebrand factor is an independent risk factor for pathogenesis of intimal hyperplasia: preliminary studies. *J. Vasc. Surg.* 37, 433–439.
- Reininger, A.J., Heijnen, H.F., Schumann, H., Specht, H.M., Schramm, W., Ruggeri, Z.M., 2006. Mechanism of platelet adhesion to von Willebrand factor and microparticle formation under high shear stress. *Blood* 107, 3537–3545.
- Rigler, R., Mets, Ü., Widengren, J., Kask, P., 1993. Fluorescence correlation spectroscopy with high count rate and low background: analysis of translational diffusion. *Eur. Biophys. J.* 22, 169–175.
- Ruggeri, Z.M., Orje, J.N., Habermann, R., Federici, A.B., Reininger, A.J., 2006. Activation-independent platelet adhesion and aggregation under elevated shear stress. *Blood* 108, 1903–1910.
- Rust, M.J., Bates, M., Zhuang, X., 2006. Sub-diffraction-limit imaging by stochastic optical reconstruction microscopy (STORM). *Nat. methods* 3, 793–795.
- Sadler, J.E., 1998. Biochemistry and genetics of von Willebrand factor. *Annu. Rev. Biochem.* 67, 395–424.
- Sadler, J.E., Budde, U., Eikenboom, J.C., Favaloro, E.J., Hill, F.G., Holmberg, L., Ingerslev, J., Lee, C.A., Lillicrap, D., Mannucci, P.M., Mazurier, C., Meyer, D., Nichols, W.L., Nishino, M., Peake, I.R., Rodeghiero, F., Schneppenheim, R., Ruggeri, Z.M., Srivastava, A., Montgomery, R.R., Federici, A.B., C. Working Party on von Willebrand Disease, 2006. Update on the pathophysiology and classification of von Willebrand disease: a report of the Subcommittee on von Willebrand Factor. *J. Thromb. Haemost.* JTH 4, 2103–2114.
- Sadler, J.E., Shelton-Inloes, B.B., Sorace, J.M., Harlan, J.M., Titani, K., Davie, E.W., 1985. Cloning and characterization of two cDNAs coding for human von Willebrand factor. *Proc. Natl. Acad. Sci. U. S. A.* 82, 6394–6398.
- Samor, B., Mazurier, C., Goudemand, M., Debeire, P., Fournet, B., Montreuil, J., 1982. Preliminary results on the carbohydrate moiety of factor VIII/von Willebrand factor (FVIII/vWF). *Thromb. Res.* 25, 81–89.
- Samor, B., Michalski, J.C., Mazurier, C., Goudemand, M., De Waard, P., Vliegthart, J.F., Strecker, G., Montreuil, J., 1989. Primary structure of the major O-glycosidically linked carbohydrate unit of human von Willebrand factor. *Glycoconj. J.* 6, 263–270.
- Schneider, S.W., Nuschele, S., Wixforth, A., Gorzelanny, C., Alexander-Katz, A., Netz, R.R., Schneider, M.F., 2007. Shear-induced unfolding triggers adhesion of von Willebrand factor fibers. *Proc. Natl. Acad. Sci. U. S. A.* 104, 7899–7903.
- Schneppenheim, R., Budde, U., 2011. Von Willebrand factor: the complex molecular genetics of a multidomain and multifunctional protein. *J. Thromb. Haemost.* JTH 9 (Suppl. 1), 209–215.
- Schneppenheim, R., Brassard, J., Krey, S., Budde, U., Kunicki, T.J., Holmberg, L., Ware, J., Ruggeri, Z.M., 1996. 'Defective dimerization of von Willebrand factor subunits due to a cys-> Arg mutation in type iid von Willebrand disease'. *Proc. Natl. Acad. Sci. U. S. A.* 93, 3581–3586.
- Shahbazi, S., Lenting, P.J., Fribourg, C., Terraube, V., Denis, C.V., Christophe, O.D., 2007. Characterization of the interaction between von Willebrand factor and osteoprotegerin. *J. Thromb. Haemost.* JTH 5, 1956–1962.
- Shelton-Inloes, B.B., Titani, K., Sadler, J.E., 1986. cDNA sequences for human von Willebrand factor reveal five types of repeated domains and five possible protein sequence polymorphisms. *Biochemistry* 25, 3164–3171.
- Solecka, B.A., Weise, C., Laffan, M.A., Kannicht, C., 2016. Site-specific analysis of von Willebrand factor O-glycosylation. *J. Thromb. Haemost.* JTH 14, 733–746.
- Spiel, A.O., Gilbert, J.C., Jilma, B., 2008. Von Willebrand factor in cardiovascular disease: focus on acute coronary syndromes. *Circulation* 117, 1449–1459.
- Sporn, L.A., Marder, V.J., Wagner, D.D., 1989. Differing polarity of the constitutive and regulated secretory pathways for von Willebrand factor in endothelial cells. *J. Cell. Biol.* 108, 1283–1289.
- Springer, T.A., 2014. Von Willebrand factor, Jedi knight of the bloodstream. *Blood* 124, 1412–1425.
- Starke, R.D., Ferraro, F., Paschalaki, K.E., Dryden, N.H., McKinnon, T.A., Sutton, R.E., Payne, E.M., Haskard, D.O., Hughes, A.D., Cutler, D.F., Laffan, M.A., Randi, A.M., 2011. Endothelial von Willebrand factor regulates angiogenesis. *Blood* 117, 1071–1080.
- Takahashi, M., Yamashita, A., Moriguchi-Goto, S., Marutsuka, K., Sato, Y., Yamamoto, H., Koshimoto, C., Asada, Y., 2009. Critical role of von Willebrand factor and platelet interaction in venous thromboembolism. *Histol. Histopathol.* 24, 1391–1398.
- Tischer, A., Campbell, J.C., Machha, V.R., Moon-Tasson, L., Benson, L.M., Sankaran, B., Kim, C., Auton, M., 2016. Mutational Constraints on Local Unfolding Inhibit the Rheological Adaptation of von Willebrand Factor. *J. Biol. Chem.* 291, 3848–3859.
- Tischer, A., Madde, P., Moon-Tasson, L., Auton, M., 2014. Misfolding of vWF to pathologically disordered conformations impacts the severity of von Willebrand disease. *Biophys. J.* 107, 1185–1195.
- Titani, K., Kumar, S., Takio, K., Ericsson, L.H., Wade, R.D., Ashida, K., Walsh, K.A., Chopek, M.W., Sadler, J.E., Fujikawa, K., 1986. Amino acid sequence of human von Willebrand factor. *Biochemistry* 25, 3171–3184.
- Tsai, H.M., 1996. Physiological cleavage of von Willebrand factor by a plasma protease is dependent on its conformation and requires calcium ion. *Blood* 87, 4235–4244.
- Valentijn, K.M., Sadler, J.E., Valentijn, J.A., Voorberg, J., Eikenboom, J., 2011. Functional architecture of Weibel-Palade bodies. *Blood* 117, 5033–5043.
- Valentijn, K.M., Valentijn, J.A., Jansen, K.A., Koster, A.J., 2008. A new look at Weibel-Palade body structure in endothelial cells using electron tomography. *J. Struct. Biol.* 161, 447–458.
- Valentijn, K.M., van Driel, L.F., Mourik, M.J., Hendriks, G.J., Arends, T.J., Koster, A.J., Valentijn, J.A., 2010. Multigranular exocytosis of Weibel-Palade bodies in vascular endothelial cells. *Blood* 116, 1807–1816.
- Verweij, C.L., Diergaarde, P.J., Hart, M., Pannekoek, H., 1986. Full-length von Willebrand factor (vWF) cDNA encodes a highly repetitive protein considerably larger than the mature vWF subunit. *EMBO J.* 5, 1839–1847.
- Vischer, U.M., Wagner, D.D., 1994. von Willebrand factor proteolytic processing and multimerization precede the formation of Weibel-Palade bodies. *Blood* 83, 3536–3544.
- Wagner, D.D., 1990. Cell biology of von Willebrand factor. *Annu. Rev. Cell. Biol.* 6, 217–246.
- Wagner, D.D., Olmsted, J.B., Marder, V.J., 1982. Immunolocalization of von Willebrand protein in Weibel-Palade bodies of human endothelial cells. *J. Cell. Biol.* 95, 355–360.
- Wienken, C.J., Baaske, P., Rothbauer, U., Braun, D., Duhr, S., 2010. Protein-binding assays in biological liquids using microscale thermophoresis. *Nat. Commun.* 1, 100.
- Ying, J., Ling, Y., Westfield, L.A., Sadler, J.E., Shao, J.Y., 2010. Unfolding of the A2 domain of von Willebrand factor with the optical trap. *Biophys. J.* 98, 1685–1693.
- Zhang, X., Halvorsen, K., Zhang, C.Z., Wong, W.P., Springer, T.A., 2009. Mechanoenzymatic cleavage of the ultralarge vascular protein von Willebrand factor. *Science* 324, 1330–1334.
- Zhao, B.Q., Chauhan, A.K., Canault, M., Patten, I.S., Yang, J.J., Dockal, M., Scheiflinger, F., Wagner, D.D., 2009. Von Willebrand factor-cleaving protease ADAMTS13 reduces ischemic brain injury in experimental stroke. *Blood* 114, 3329–3334.
- Zhou, Y.F., Eng, E.T., Nishida, N., Lu, C., Walz, T., Springer, T.A., 2011. A pH-regulated dimeric bouquet in the structure of von Willebrand factor. *EMBO J.* 30, 4098–4111.
- Zhou, Y.F., Eng, E.T., Zhu, J., Lu, C., Walz, T., Springer, T.A., 2012. Sequence and structure relationships within von Willebrand factor. *Blood* 120, 449–458.
- Zhou, Y.F., Springer, T.A., 2014. Highly reinforced structure of a C-terminal dimerization domain in von Willebrand factor. *Blood* 123 (12), 1785–1793.
- Zucker, M.B., Broekman, M.J., Kaplan, K.L., 1979. Factor VIII-related antigen in human blood platelets: localization and release by thrombin and collagen. *J. Lab. Clin. Med.* 94, 675–682.